PHYSICAL REVIEW B **78**, 035305 (2008)

Formation of epitaxial gold nanoislands on (100) silicon

Emanuela Piscopiello* and Leander Tapfer
Department of Advanced Physics Technology and New Materials (FIM), ENEA, Strada Statale 'Appia', Brindisi, I-72100, Italy

Marco Vittori Antisari
Department of Advanced Physics Technology and New Materials (FIM), ENEA, via Anguillarese 301, Roma, I-00060, Italy

Pasquale Paiano
CNISM-Research Unit of Lecce and Department of Innovation Engineering, University of Salento, via Arnesano, Lecce, I-73100, Italy

Paola Prete
Institute for Microelectronics and Microsystems (IMM), CNR, via Arnesano, Lecce, I-73100, Italy

Nicola Lovergine
CNISM-Research Unit of Lecce and Department of Innovation Engineering, University of Salento, via Arnesano, Lecce, I-73100, Italy
(Received 7 February 2008; revised manuscript received 12 May 2008; published 2 July 2008)

Coherent gold nanoislands were prepared directly on (100)-oriented Si substrates by a physical methodology, consisting of the thermal evaporation of a very thin Au film ($t \sim 2$ nm) and its successive annealing in the temperature range 350 °C$<T<$814 °C. We found that at annealing temperature of 814 °C and in the presence of residual oxygen during the annealing process, epitaxial monocrystalline gold nanoislands embedded in the Si lattice are formed. The crystallographic orientation and epitaxial relationship between the Au nanoislands and the Si lattice are well defined. In contrast, at lower annealing temperatures, namely at 350 °C and 626 °C, the nanoislands are randomly oriented without epitaxial relationships. The morphology, orientation, and crystalline structure of Au nanoislands were investigated by scanning and high-resolution transmission electron microscopy and grazing-incidence x-ray diffraction. A model of the epitaxial Au nanoisland formation on (100)Si is presented in which the Si-atom out-diffusion and the formation of a liquid Au-Si droplet during the annealing process (increasing temperature) and the Si redeposition and oxidation (i.e., SiO_x complex formation and removing of the excess Si in the gold islands) during the cooling process (decreasing temperature) play a fundamental role.

DOI: 10.1103/PhysRevB.78.035305 PACS number(s): 68.35.Fx, 61.05.C−, 61.46.−w, 68.37.Lp

I. INTRODUCTION

The controlled self-assembly of metal nanoparticles on semiconductor and oxide surfaces is a research topic of very great current interest. The organization of nanometer-scale metal objects on larger objects, such as semiconductor substrates, allows to better exploit the nanoparticle properties and to fabricate novel and larger integrated devices. The interest is driven by scientific aspects, in particular due to the unique electronic, magnetic, photonic and catalytic properties of metal nanoparticles, and by nanotechnological aspects related to the preparation of new materials for energy, photonics, communications, and sensing applications.[1–5]

In particular, gold clusters and nanoislands dispersed on semiconductor surfaces attract great attention due to the catalytic, electronic, and optical properties of nanosized gold crystals[6,7] and the possibility to functionalize them with organic molecules.[8,9] For example, DNA functionalization and subsequent hybridization of Au nanoparticles immobilized onto Si substrates can be exploited to fabricate specific biosensor devices in solid phase.[10]

Furthermore, gold nanoislands are extensively used as metal catalyst for the synthesis of one-dimensional (1D) semiconductor nanostructures by employing advanced epitaxial growth techniques, such as molecular beam epitaxy[11] and metal-organic vapor-phase epitaxy (MOVPE).[12,13] Vertically aligned semiconductor nanowires[14–17] and single-wall carbon nanotubes[18] were successfully fabricated by Au-assisted growth. These nanostructures offer an ideal basis to investigate the 1D quantum confinement effects and to explore their possible applications in the next generation of nanoelectron devices.[19–21]

In many of these experiments and studies Si wafers were employed as substrates, because silicon is the paramount substrate material for electronic devices that allows to use the well- established process technology and an easy integration in and with other device structures becomes feasible.

Different methods have been used to produce gold nanoparticles or nanoislands on silicon substrates. Thiol-capped Au nanoparticles are prepared by a wet chemical synthesis procedure and are subsequently dispersed on Si surface and the organic residues are removed by UV light exposure[22] or O^+-plasma treatment.[8,23] More frequently, magnetron sputtering, thermal and *e*-beam evaporation methods combined with post-deposition thermal annealing processes were used to fabricate gold islands and particles on Si.[24,25] It was found that the wetting and the gold island formation on Si substrates may depend on the gold film deposition method and silicon surface preparation.[26]

Here, the gold particle/island formation on silicon is related to the particular properties of the Si/Au interface, i.e., surface diffusion of Au on Si2[24,25,27,15] and Si/Au

 ©2008 The American Physical Society

interdiffusion,[28–30] and to the eutectic alloy formation.[24,31] Recently, Hannon *et al.*[15] have demonstrated that, in the case of the Au-catalyzed growth of silicon nanowires on Si(111), Au surface diffusion during growth determines the length, shape, and sidewall properties of the nanowires. Gold from the catalyst droplets wets the nanowire sidewalls, eventually consuming the droplets and terminating the vapor-liquid-solid (VLS) growth. Gold atoms migrating from the smaller to the larger droplets, through the mechanism of Ostwald ripening, lead to nanowire diameters that change during growth. Interdiffusion at the Au-Si interface occurs even at room temperature.[28,30] The Si diffusion into the gold layer is necessary to form an eutectic alloy, yet at the eutectic temperature the diffusivity of Au into silicon is not sufficient to form an alloy droplet.[24] The Au-Si eutectic formation and the evolution and dynamics of μm- and sub-μm-sized islands on Si surfaces during the thermal annealing processes were investigated by several research groups.[24–27,31] It was reported that gold islands can be formed by thermal annealing already at temperatures below 200 °C,[32,33] which is much lower than the melting temperature of bulk gold (1300 °C).

In this work, we present results on the formation of nm-sized gold islands onto Si substrates by thermal evaporation of a thin Au film and its successive annealing at different temperatures (temperature range between 350 °C and 814 °C). In particular, we show that at annealing temperature $T=814$ °C, the Au nanostructures are monocrystalline lens-shaped islands and are embedded in the Si lattice with a well-defined crystallographic orientation and epitaxial relationships between the Au and Si lattices.

This paper is organized as follows: The experimental details of the Au nanoisland fabrication on Si surfaces and the methods and procedures of the microstructural analysis are described in Sec. II; the results of the microstructural investigations are reported and discussed in Sec. III. In particular, Sec. III A reports on the morphology and structure of the Au nanoislands and in Sec. III B the epitaxial relationship of the Au nanoislands with the Si lattice is presented. In Sec. III C a model for the embedded Au nanoisland formation is proposed.

II. EXPERIMENT

Au nanoislands were self-assembled on p-type (100)Si substrates cleaved from commercial wafers. The substrate was sonicated in iso-propanol for 1h in order to remove the organic contaminants, subsequently etched in $NH_4F:HF$ solution for 6 min at room temperature removing the thin native-oxide surface layer, rinsed in deionized water, dried under pure N_2 and, finally, loaded into a Joule evaporator UHV chamber for the Au thin-film deposition. The evaporation rate was 0.02 nm/s and the final gold film thickness was ~2 nm. In order to obtain the Au nanoparticles the Au/(100)Si sample was then loaded into the quartz chamber of a horizontal tubular resistance furnace for a thermal treatment in a 6N pure nitrogen atmosphere. The annealing was performed for 20 min. at different temperatures in the range between 350 °C and 814 °C under a N_2 flow of 130 cm^3/min. Higher annealing temperatures were not considered for our experiments because gold evaporation occurs at temperatures above 850 °C.[24] The temperature was increased from RT to the final value at a rate of about 10 °C/sec. This treatment allows the Au thin film to self-assemble into a dense and uniform array of nanoparticles across the silicon substrate surface.

The morphologies of both the as-deposited and the annealed Au thin film were analyzed by field-emission scanning electron microscopy (FE-SEM) observations using a JEOL microscope model JSM 6500F. The morphology, size, and crystalline structure of the self-assembled Au nanoislands were characterized by conventional (CTEM) and high-resolution transmission electron microscopy (HRTEM) and by x-ray diffraction (XRD). CTEM and HRTEM observations were performed by using a TECNAI F30 transmission electron microscope operating at 300 kV and with a point-to-point resolution of 0.205 nm. Transmission electron microscopy (TEM) cross-sectional specimens were prepared by conventional mechanical polishing up to a thickness of about 20 μm, followed by glazy angle ion beam milling up to electron transparency thickness, in a Gatan Precision Ion Polishing System (PIPS).

XRD measurements were performed in both Bragg (θ-2θ scan) and glancing incidence (GIXD) geometry by using the K_α-lines of both Cu and Co radiation ($l_{Cu}=0.1540562$ nm and $l_{Co}=0.178892$ nm). GIXD spectra were recorded by using a high-resolution x-ray diffractometer (HRD3000 Ital-Structures) in parallel beam optic configuration (Max-Flux Optical System). The GIXD configuration is particularly indicated to reveal and investigate very thin surface layers and near-surface structures due to the reduced x-ray penetration depth at glancing incidence conditions. These measurements were obtained by a 2θ-scan and keeping the angle between the incident x-ray beam and the sample surface constant at $\omega=1.0°$.

III. RESULTS AND DISCUSSION

A. Morphology and structure of the Au nanoisland

FE-SEM observations, carried out in the secondary electron detection mode, of the as-deposited thin films evidence the granular and porous gold surface morphology [Fig. 1(a)]: The noncontinuous cellular structure of the thin Au film deposited on silicon is due to the nonwetting nature of Au.[24,25,34] After the thermal treatment at 814 °C Au nanoislands are formed as shown in the FE-SEM micrograph in Fig. 1(b). Here, the average lateral island size is about 15–20 nm. The shape and size of the nanoislands change very little with the annealing temperature within the interval investigated (350 °C$<T_A<$814 °C), yielding slightly larger islands at higher temperature. Between the Au islands (bright areas) also small zones of faint contrast can be observed and are associated with very shallow pits probably generated during the very initial annealing process and the Au islands formation (Ostwald ripening).

The structural properties of the as-deposited and annealed Au films were analyzed by GIXD measurements using the coplanar diffraction scheme shown in Fig. 2. The angle ω between the incident beam $\vec{k}_0$ and the (100)Si was kept con-

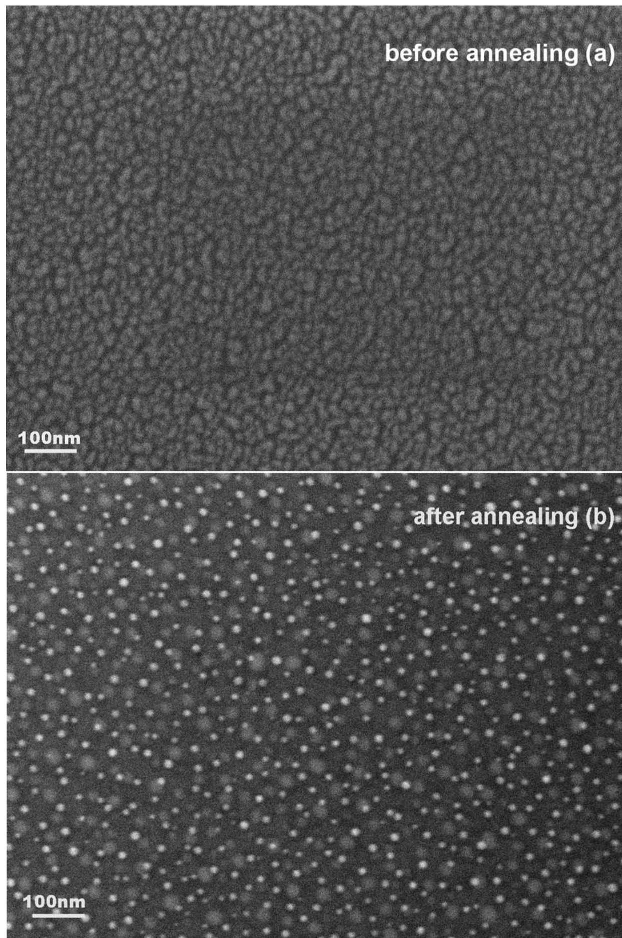

FIG. 1. (a) FE-SEM micrographs of the as-deposited Au film (2 nm) on (100)Si substrate (a) and after the annealing at 814 °C for 20 min. (b). The as-deposited film shows a cellular structure due to the nonwetting nature of gold on silicon.

stant ($\omega=1°$) while the intensity of the scattered beam $\vec{k}_h$ was recorded by moving the detector by angle 2θ. The GIXD patterns of the as-deposited and annealed Au films are shown in Fig. 3. In order to avoid the contribution of the Si substrate, particularly the (311) Bragg reflection, the samples

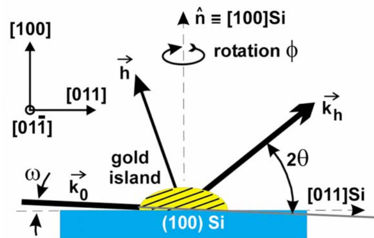

FIG. 2. (Color online) Scheme of the coplanar grazing-incidence x-ray diffraction configuration. The diffraction patterns were recorded by keeping the angle ω between the incidence beam $\vec{k}_0$ and the (100)Si surface constant while the intensity of the scattered beam $\vec{k}_h$ was recorded by moving the detector by 2θ. GIXRD patterns for different φ-angle settings were recorded (rotation by angle φ around the (100)Si normal $\hat{n}$). Here, the crystallographic reference system refers to the Si substrate wafer with $\varphi=0$.

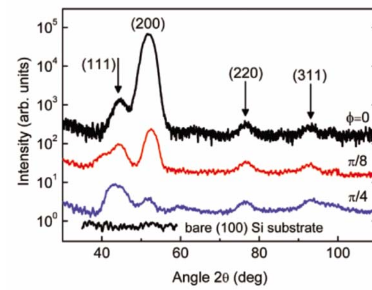

FIG. 3. (Color online) GIXRD patterns on the as-deposited (curve A) and the Au films annealed at $T=350$ °C (curve B), 626 °C (curve C), and 814 °C (curve D), respectively. The 2θ scans were recorded at fixed incidence angle $\omega_i=1.0°$ and by using CuK_a-radiation. The patterns show the typical Au peaks for the as-deposited and annealed ($T<626$ °C) samples, while the Au film annealed at 814 °C exhibits a single, very intense (111)Au peak indicating a pronounced texture.

were rotated around the normal axis $\hat{n}$ by an angle of $\varphi=\pi/8$ ($\varphi=0$ corresponds to the configuration where the (011)Si axis is parallel to the scattering plane). The diffraction pattern of the as-deposited Au film (curve A) shows the most intense Au Bragg peaks as expected for a polycrystalline film. The relative intensity of the measured Bragg peaks are in accordance with the crystallographic powder database (PDF #04–0784).[35] No appreciable changes can be noticed in the GIXD patterns of the samples annealed at 350 °C (curve B) and 626 °C (curve C) suggesting a random crystallographic orientation of the Au nanoislands. However, the GIXD pattern of the sample annealed at 814 °C shows only a very intense (111)Au Bragg peak while all other Bragg peaks are not observed.

In order to investigate more accurately the crystallographic orientation of the Au nanoislands, additional GIXD patterns (Co radiation) were recorded for different φ-angles in the range between 0 and 2π and with incremental step $\Delta\varphi=n\times\frac{\pi}{8}$ corresponding to rotation of the sample around the (100)Si normal. For these experiments a different x-ray radiation wavelength (Co radiation) was used in order to avoid the excitation of the (311)Si reflection of the Si substrate that occurs at the glancing incidence conditions and the angle settings of $\varphi=n\times\frac{\pi}{4}$, and, therefore, would hide the main Au Bragg peaks. Figure 4 shows the GIXD patterns for the angles $\varphi=0$, $\pi/8$ and $\pi/4$; $\varphi=0$ corresponds to the sample setting where the (011)Si axis is parallel to the x-ray scattering plane. In Fig. 4 the GIXD pattern recorded from a bare (100)Si substrate is also shown as reference signal. For the case $\varphi=0$ a very intense (200)Au peak is observed, while all the other peaks are several orders of magnitude lower in intensity; it should also be noted that for the equivalent settings $\varphi=\pi/2$, π, and $3\pi/2$ the same GIXD pattern was obtained. However, the situation changes dramatically for the other φ-angle settings (i.e., $\varphi=\pi/8$ and $\pi/4$) where the intensity of (200)Au peak is much reduced as shown in Fig. 4, indicating that the (200)Au planes no longer satisfy the ideal diffraction condition.

These results indicate a well-defined crystallographic orientation of the Au nanoislands with respect to the Si lattice.

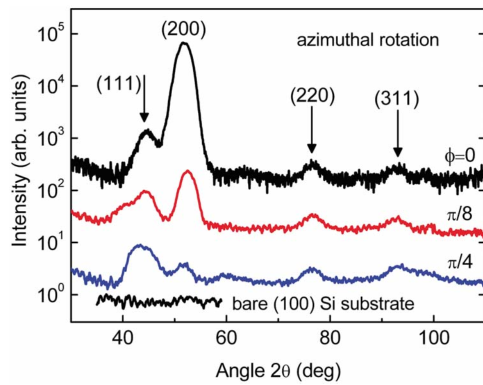

FIG. 4. (Color online) GIXRD patterns of the Au film annealed at 814 °C obtained for different φ angles (φ=0, $\pi/8$ and $\pi/4$) by using CoK_α-radiation and keeping the incidence angle constant ω_i =1.0°. As a reference, the diffraction pattern of the bare Si substrate is also shown. For φ=0 (in this setting the (011)Si planes are normal to the scattering plane) a very intense (200)Au peak is observed, while all other peaks are very weak (note the logarithmic intensity axis).

Indeed, only for well-defined settings of the rotation (φ) and incident (ω) angles are the (111)Au (see Fig. 3) and (200)Au (see Fig. 4) peaks well observed. A quantitative analysis of the diffraction profiles allows us to estimate the size (lattice coherence) of the Au nanoislands along the diffraction vector that corresponds to an island size (in this case is equivalent to the height of the nanoislands) of about 4 to 5 nm.

The microstructure of the Au nanoislands and their crystallographic relationship with the Si lattice and the Au/Si interfaces have also been analyzed by high-resolution TEM observations of the annealed samples. Figure 5 shows the TEM cross-sectional views of the samples annealed at 350 °C (a) and 814 °C (b), respectively. Similar results were also obtained from TEM observations of the sample annealed at 626 °C (not shown here). The Au nanoislands (darker contrast) on top of the Si substrate are well-observed in all cases. The nanoislands have an elongated shape (up to about 20 nm) in the direction parallel to the Si surface. Furthermore, the nanoislands are embedded in the Si substrate and a faceting at the Si-Au interface can be noticed. This faceting is well observed for the sample annealed at higher temperature (814 °C) where the nanoislands are much larger in size and their size distribution is also more uniform. In fact, due to Ostwald ripening phenomenon with increasing annealing temperature the average nanoisland size increases while the density is reduced. In order to better evidence this faceting, one of the nanoislands is shown in a magnified view in the inset of Fig. 5(b) and its facets are evidenced (red lines); these facets correspond to the (111), (311) and (711) lattice planes of Si.

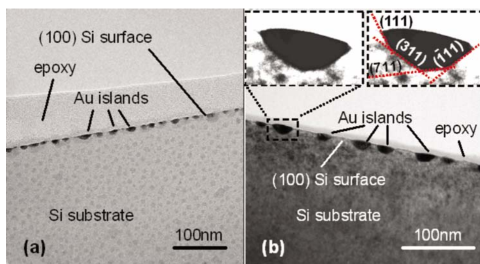

FIG. 5. (Color online) Bright field cross-sectional TEM images of the samples annealed at 350 °C (a) and 814 °C (b), respectively. Au nanoislands grown on clean (100)Si substrate are well-visible on top of the surface (darker contrast). The thin layer, visible on top of Au nanoparticles, is the residual glue used for TEM sample preparation. With increasing annealing temperature the island size is increased while the density is reduced in accordance with the Ostwald ripening phenomenon. The insets in image (b) show an enlarged single Au NP with well-defined facets (left inset) that correspond to the (111), (311), (711) and (−111) Si planes marked by dotted lines (right inset).

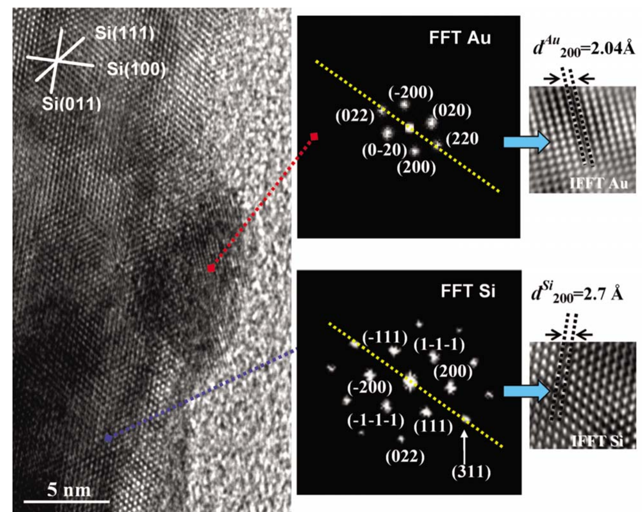

FIG. 6. (Color online) HRTEM image of an Au nanoisland directly grown on clean Si surface after annealing at 814 °C. On the right-hand side the corresponding FFT patterns taken from the regions of the Au island and Si substrate (indicated by the red and blue arrows, respectively) and the filtered images (IFFT=Inverse fast Fourier transform) of the crystalline structures of Au and Si, respectively, are shown. These results reveal the following Au-Si lattice relationships: 001 Au∥[0−11]Si and [220]Au∥[311]Si. In the FFT patterns, the dotted lines (yellow color) highlight the last relation existing between the Au and the Si lattices.

A HRTEM image of a single Au nanoisland is shown in Fig. 6. The lattice planes of Au and Si as well as the facetted Au-Si interface are well observed in this image. In addition to this, no extended defects or clustering phenomena are revealed at the Au-Si interface or within the Au nanoislands. Furthermore, the HRTEM images show that the Au/Si interface is flat on the atomic scale and no amorphous interlayer is found next to it.

A fast Fourier transform (FFT) analysis of the HRTEM images (Fig. 6, right side) demonstrates that the Au nanoislands are monocrystalline, and the following epitaxial relationships hold between the Au and Si lattices: [001]Au∥[0$\bar{1}$1]SI and [220]Au∥[311]Si. The dotted lines (yellow color) in the FFT patterns highlight the [220]Au∥[311]Si relation existing between the Au and the Si lattices. The d-spacing for the (200) planes of the Au island and the Si wafer are also reported.

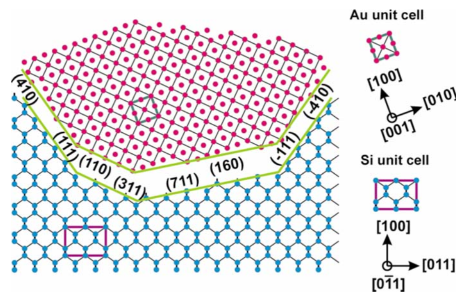

FIG. 7. (Color online) Scheme of the Au island embedded in (100)Si showing the Au lattice accommodated to the Si near-surface lattice. The (100)Au planes are parallel to the (311)Si planes, i.e., the Au lattice is rotated by about 21° with respect to the Si lattice, as evidenced from the HRTEM and GIXRD measurements. In this configuration the lattice mismatch between the two crystals is minimized.

B. Origin of the Au nanoisland / Si lattice epitaxial relationships

The GIXD and TEM results suggest that there is an epitaxial relationship between the Au and Si lattices inspite of the huge lattice mismatch of about 25%. A scheme of the Au lattice accommodated to the surface of the Si crystal is reported in Fig. 7. The geometrical configuration of the two lattices in the scheme is the same as for the TEM images in Fig. 6, i.e., the Si lattice is viewed along one of its $[0\bar{1}1]$ direction, while the Au lattice along its 001-direction. Furthermore, the (110)Au planes are set parallel to the (311)Si planes, i.e., the Au lattice is rotated by about 21° with respect to the Si lattice, as evidenced experimentally by the FFT TEM images in Fig. 6. In this way the (111) and (711) planes of the Si are found to be almost parallel to the (410) and (160) planes of Au, respectively. This epitaxial configuration reduces the lattice mismatch between the two crystal lattices: A lattice mismatch of about-3.9%+3.6% and-6.0% for the (110)Au‖(311)Si, (160)Au‖(711)Si and (410)Au‖(111)Si interface planes, respectively, is obtained. These findings can be well explained by lattice-constant-adaptable crystallographic considerations.[36] Hence, the specific Au/Si interfaces allow to reduce the lattice mismatch between the two lattices and to form crystallographic coherent Au nanoislands on the Si surface. Therefore, the shape and morphology of the islands are a consequence of the specific epitaxial relations between the Au nanoislands and the Si substrate.

C. Epitaxial Au nanoisland formation model

The Au-Si system, specifically the Au-silicide formation and Au/Si diffusion mechanisms, have been investigated for several decades due to the importance of gold in Si-based microelectronics. Thus, it is well known that Si diffuses rapidly through evaporated gold films, even at room temperature, provided that there is no SiO_2 interlayer between Si substrate and gold film that acts as a barrier layer for the diffusion of Si.[27,30,37]

In addition, while, for most systems the liquid and solid are usually nonmiscible, Au is reactive and dissolves silicon to form a liquid. The melting temperature of pure gold (bulk) is 1064 °C, however, the bulk Au-Si phase diagram exhibits a eutectic point with a eutectic temperature and composition of 363 °C and 19 at.% Si.[38] For nanoparticles a lowering of the eutectic temperature was observed recently: The phase diagram for Au-Si droplets with $\emptyset=10$ nm shows a eutectic point with a temperature and composition of about 300 °C and[17] at.% Si.[39] No Au-Si compounds are formed and the only phases present are the liquid and the Si and Au solid phases with low mutual solid solubility.[24,31]

If the thin gold film deposited on the Si substrate is annealed at temperatures above 200 °C [32,33] Au/Si droplets are formed because of surface tension. The mobility of the Au at the surface increases with temperature and larger droplets grow at the expense of the smaller ones (Ostwald ripening). Simultaneously, Si atoms diffuse into the Au islands forming a liquid Au-Si droplet in equilibrium. With increasing the temperature further Si atoms diffuse from the substrate in the droplets and the Si concentration in the liquid droplets increases following the liquidus curve in the Au-Si phase diagram. As observed by Ressel *et al.*[24] the Si concentration of the droplet-surfaces does not correspond to the bulk liquid composition as expected from the phase diagram, but instead the surface is highly Si-enriched. In addition, a phase separation was observed.

In order to prevent gold evaporation during our annealing experiments the annealing temperature was kept below 850 °C. In fact, at higher temperatures (~1000 °C) other phenomena such as the solid-liquid-solid mechanism of growth that leads to silicon nanowire growth without vapor-phase reactants, may occur.[40]

In our experiments the annealing process is carried out under a flow of N_2 gas, but residual O_2 is still present as revealed by quadrupole ion mass spectrometry measurements. The presence of residual oxygen in the quartz chamber during the annealing process is crucial for our experimental results. The residual oxygen may interact with the Si on top of the Au-Si droplets forming SiO and/or SiO_2 molecules. In order to keep the Si concentration in the droplets constant, more Si diffuses from the substrate into the droplets in accordance with the equilibrium condition described by the phase diagram. As long as the temperature is kept constant this process may continue and more Si diffuses from the substrate into the Au-Si in order to ensure that the droplets are saturated with Si and, consequently, this may lead to the observed phenomenon that the droplets sink into the Si wafer, i.e., the droplets are embedded into the Si substrate (dissolution of Si).

Upon cooling, the droplets are supersaturated with Si and a segregation of Si on the droplet surface and a phase separation of Si and Au occur. But at the same time Si atoms are also deposited, under the droplets, on the Si substrate.[24] The dissolution and deposition may also lead to the surface migration of the droplets that has been observed and already reported in literature.[17,24,27] However, in our case, the dynamic mechanism of Si dissolution and oxidation—that leads to the embedded droplets—may prevent or hinder the migration of the droplets. The Si will be partly oxidized and partly deposited at the substrate/droplet interface.

If the sample is further cooled down, below the eutectic point, the droplets crystallize and form Au nanoislands that

are embedded in the Si lattice according to the epitaxial relationships and minimizing the lattice mismatch, as observed and measured in our TEM and GIXD experiments.

It is interesting to note that the formation of stress-free particles with crystallographic facets were observed after indiffusion of gold in crystalline silicon at high temperatures for a long period of time (from several hours to days).[41] In these diffusion experiments gold precipitates in silicon and forms nanometer-sized gold silicide clusters that are embedded stress-free into the silicon matrix and are delimited (confined) by crystallographic planes of the silicon lattice. It was argued that these crystallographic planes minimize the stress and interface energy between particles and matrix.

IV. CONCLUSIONS

We report on the formation of monocrystalline epitaxial gold nanoislands on (100)Si surfaces. The nanoisland formation was obtained by thermal evaporation of a few nanometer thick Au film and its successive thermal annealing in N_2 atmosphere.

We found that the gold nanoislands annealed at temperatures below 800 °C (350 °C and 626 °C) are randomly oriented. However, a well-defined crystallographic orientation of the nanoislands was observed at $T=814°$. The orientation, structure, and morphology of the nanoislands are investigated by grazing-incidence x-ray diffraction and transmission electron microscopy. We found that the nanoislands have a lens-like shape of lateral size and thickness of about 30 nm and 5 nm, respectively. The nanoislands are embedded in the silicon wafer and exhibit a pronounced epitaxial relationship. Well-defined smooth Au-Si interface facets are formed: The (111), (311) and (711) planes of the Si are found to be almost parallel to the (410), (110) and (160) planes of Au, respectively. As a consequence, the gold lattice cell is rotated by 45° and tilted by 21° with respect to the Si lattice. The formation of these particular interfaces minimizes the huge lattice mismatch between gold and silicon (25%) in accordance with lattice-constant-adaptable crystallographic considerations. The reduced lattice mismatch for these interface configurations (about 4%) and the small size of the nanoislands allow an elastic relaxation of the strain field. Hence, it is possible that coherent epitaxial gold nanoislands are formed and embedded in the silicon lattices, without lattice defects at the gold/silicon interface as shown by high-resolution TEM.

The generation of the buried nanoislands are explained by the liquid alloy droplet formation close to the Au-Si eutectic temperature and the Si diffusion in the gold droplets at higher temperature. The presence of residual oxygen in the N_2 atmosphere during the annealing process leads to oxidation of the Si on the surface of the droplets, and in order to keep the Si concentration in the droplets constant, more Si atoms diffuse from the substrate into the droplets in accordance with the equilibrium condition (Au-Si phase diagram). This process leads finally to the observed phenomenon that the droplets sink into the Si wafer, i.e., the droplets are embedded into the Si substrate. By reducing the annealing temperature, the droplets are supersaturated with Si and a redeposition of Si occurs. During this last step of the process, coherent Au-Si interfaces are formed with well-oriented and coherent gold nanoislands embedded in the Si.

The formation of coherent epitaxial gold nanoislands—all having the same crystallographic orientation and without lattice defects—"anchored" in the Si lattice, as described here, constitutes an easy self-assembling nanocrystal fabrication process that would be of great interest and importance for the catalytic vapor-phase growth of nanorods and nanowires, but this could also be of remarkable relevance for the design and realization of novel nanosensor devices exploiting the enhanced physical, chemical, and catalytic properties of the nanosized gold.

---

*Corresponding author.emanuela.piscopiello@brindisi.enea.it

[1] B. C. Gates, Chem. Rev. (Washington, D.C.) **95**, 511 (1995).
[2] H.-J. Freund, Surf. Sci. **500**, 271 (2002).
[3] C. Burda, X. Chen, R. Narayanan, and M. A. El-Sayed, Chem. Rev. (Washington, D.C.) **105**, 1025 (2005).
[4] R. Burch, Phys. Chem. Chem. Phys. **8**, 5483 (2006).
[5] S. W. Boettcher, N. C. Strandwitz, M. Schierhorn, N. Lock, M. C. Lonergan, and G. D. Stucky, Nat. Mater. **6**, 592 (2007).
[6] S. Link and M. A. El-Sayed, Int. Rev. Phys. Chem. **19**, 409 (2000); T. Lee, J. Liu, N. P. Chen, R. P. Andres, D. B. Janes, and R. Reifenberger, J. Nanopart. Res. **2**, 345 (2000).
[7] E. Roduner, Chem. Soc. Rev. **35**, 583 (2006).
[8] J. Ch. Love, L. A. Estroff, J. K. Kriebel, R. G. Nuzzo, and G. M. Whitesides, Chem. Rev. (Washington, D.C.) **105**, 1103 (2005).
[9] W. Fritzsche and T. A. Taton, Nanotechnology **14**, R63 (2003).
[10] J. Spadavecchia, P. Prete, N. Lovergine, L. Tapfer, and R. Rella, J. Phys. Chem. B **109**, 17347 (2005).
[11] Z. H. Wu, X. Y. Mei, D. Kim, M. Blumin, and H. E. Ruda, Appl. Phys. Lett. **81**, 5177 (2002).
[12] K. Hiruma, M. Yazawa, T. Katsuyama, K. Ogawa, K. Haraguchi, M. Koguchi, and H. Kakibayashi, J. Appl. Phys. **77**, 447 (1995).
[13] Q. X. Liu, C. X. Wang, N. S. Xu, and G. W. Yang, Phys. Rev. B **72**, 085417 (2005).
[14] F. M. Ross, J. Tersoff, and M. C. Reuter, Phys. Rev. Lett. **95**, 146104 (2005).
[15] J. B. Hannon, S. Kodambaka, F. M. Ross, and R. M. Tromp, Nature (London) **440**, 69 (2006).
[16] W. Seifert, M. Borgström, K. Deppert, K. A. Dick, J. Johansson, M. W. Larsson, T. Mårtensson, N. Sköld, C. P. T. Svensson, B. A. Wacaser, L. R. Wallenberg, and L. Samuelson, J. Cryst. Growth **272**, 211 (2004).
[17] P. Paiano, P. Prete, E. Speiser, N. Lovergine, W. Richter, L. Tapfer, and A. M. Mancini, J. Cryst. Growth **298**, 620 (2007).
[18] D. Takagi, Y. Homma, H. Hibino, S. Suzuki, and Y. Kobayashi, Nano Lett. **6**, 2642 (2006).
[19] S. J. Tans, A. R. M. Verschueren, and C. Dekker, Nature (London) **393**, 49 (1998); R. Martel, T. Schmidt, H. R. Shea, T. Hertel, and Ph. Avouris, Appl. Phys. Lett. **73**, 2447 (1998).

[20] Y. Cui and C. M. Lieber, Science **291**, 851 (2001).
[21] K. Terabe, T. Hasegawa, T. Nakayama, and M. Aono, Nature (London) **433**, 47 (2005).
[22] S. Sun, P. Mendes, K. Critchley, S. Diegoli, M. Hanwell, S. D. Evans, G. J. Leggett, J. A. Preece, and T. H. Richardson, Nano Lett. **6**, 345 (2006).
[23] K. Raiber, A. Terfort, C. Benndorf, N. Krings, and H.-H. Strehblow, Surf. Sci. **595**, 56 (2005).
[24] B. Ressel, K. C. Prince, S. Heun, and Y. Homma, J. Appl. Phys. **93**, 3886 (2003).
[25] A. I. Oliva, J. L. Sacedon, E. Anguiano, M. Aguilar, J. A. Aznarez, and J. A. Mendez, Surf. Sci. **417**, L1139 (1998).
[26] B. Lamontagne, E. Sacher, and M. R. Wertheimer, Appl. Surf. Sci. **64**, 205 (1993).
[27] J. Slezak, M. Ondrejcek, Z. Chvoj, V. Chab, H. Conrad, S. Heun, Th. Schmidt, B. Ressel, and K. C. Prince, Phys. Rev. B **61**, 16121 (2000).
[28] A. K. Green and E. Bauer, J. Appl. Phys. **47**, 1290 (1976).
[29] D. Mathiot, Phys. Rev. B **45**, 13345 (1992).
[30] J. K. Bal and S. Hazra, Phys. Rev. B **75**, 205411 (2007).
[31] O. G. Shpyrko, R. Streitel, V. S. K. Balagurusamy, A. Y. Grigoriev, M. Deutsch, B. M. Ocko, M. Meron, B. Lin, and P. S. Pershan, Science **313**, 77 (2006).
[32] W. Swiech, E. Bauer, and M. Mundschau, Surf. Sci. **253**, 283 (1991).
[33] T. F. Young, J. F. Chang, and H. Y. Ueng, Thin Solid Films **322**, 319 (1998).
[34] T. Nagao, S. Hasegawa, K. Tsuchie, S. Ino, C. Voges, G. Klos, H. Pfnür, and M. Henzler, Phys. Rev. B **57**, 10100 (1998).
[35] Joint Committee on Powder Diffraction Standards-International Centre for Diffraction Data (JCPDS-ICDD), Newtown Square, PA, 2000.
[36] J. Haisma, J. A. Pistorius, and D. Mateika, J. Cryst. Growth **102**, 979 (1990).
[37] C. A. Hewett and S. S. Lau, Appl. Phys. Lett. **50**, 827 (1987).
[38] *Physical Chemistry: Thermodynamic Properties of Inorganic Materials*, Landolt-Börnstein, New Series, Group IV Vol. 19, Pt. B1, edited by W. Martienssen (Springer, Berlin, 2002), p. 296.
[39] D. Bahloul-Hourlier and P. Perrot, J. Phase Equilib. **28**, 150 (2007).
[40] M. Paulose, O. K. Varghese, and C. A. Grimes, J. Nanosci. Nanotechnol. **3**, 341 (2003).
[41] F. H. Baumann and W. Schröter, Phys. Rev. B **43**, 6510 (1991).